Numerical investigation of UF membrane to reduce energy consumption using double porosity approach

S. Ghotbi, B. Pirzadeh, Davod Mohebbi-Kalhori and A. Abdollahi

ABSTRACT

Hollow fiber (HF) membranes with circular geometry, are used in many separation processes such as water and wastewater treatment. Since optimization of energy efficiency is important for wastewater treatment, the aim of this study was to investigate the effect of non-circular geometry of the inner surface of the HF on the separation performance. To this purpose, the HF bundle has been assumed as a double porous media having two porosities and permeabilities. Since these two parameters are defined by the geometry of the porous medium, any change in the geometry affects their values and the media performance. Therefore, in this study a mathematical modeling has been divided into five categories, including circular, oval, square, rectangular and triangular geometries, and their geometric properties have been calculated based on three different strategies. The results have been compared with the data obtained from literature and showed that the membrane inner surface to cross-section area ratio (*a*), axial permeability, and porosity in the inner region for the non-circular HF are larger than that of the circular HF and *a* increased 16%, 27%, 35% and 65% in ellipse, square, rectangle and triangle geometry, respectively, in comparison with the circle. Axial permeability increased 98%, 68%, 63%, and 26% for a triangle, rectangle, ellipse, and square respectively in the third strategy when compared to the circle. Due to 50% feed flow rate reduction, maximum transmembrane pressure (TMP) reduction was 85% related to the rectangular geometry in the first strategy and minimum was 55% corresponding to the triangle in the third strategy. As *a* increased up to 65%, TMP reduced by up to 200% and consequently energy consumption and operating costs of the system are decreased.

Key words | cross-sectional geometry, double porous media, energy consumption, hollow fiber, TMP, wastewater

S. Ghotbi
B. Pirzadeh (corresponding author)
A. Abdollahi
Department of Civil Engineering,
University of Sistan and Baluchestan,
Zahedan,
Iran
E-mail: *b_pirzadeh@eng.usb.ac.ir*

Davod Mohebbi-Kalhori
Department of Chemical Engineering,
University of Sistan and Baluchestan,
Zahedan,
Iran

INTRODUCTION

When water shortages arise, the three main sources considered are; water conservation, water recycling, and desalination. Because water conservation has its limitations, the most effective alternatives to obtain water resources are the water recycling and desalination in terms of price. In this regard, the use of membranes is the best solution (EPA 2005). Among the different polymeric membranes, hollow fiber (HF) membranes are used in several processes, such as water and wastewater treatment. Numerous studies have been done to better understand the fiber production with a higher performance (Widjojo & Chung 2006; Jiang *et al.* 2008; Arthanareeswaran *et al.* 2010; Deng *et al.* 2011; Wan *et al.* 2017). The advantage of these membranes is their larger inner surface to cross-section ratio. In all applications that perform with these membranes, the fibers are circular cylindrical shape, but the reason for choosing this geometry is not the maximum inner surface area per unit cross-section ratio of the membrane but rather the existing methods of manufacture. The external or internal circular shape of the fibers can be changed to improve the surface area. It also reduces the module production cost significantly, which is highly desired. A few researchers (Buer & Cumin 2010; Culfaz *et al.* 2011a) investigated the fouling resistance of non-circular HFs in constant flux experimentally. Their results showed that the fouling resistance for these fibers increases more rapidly than the circular fibers and fouling has better reversibility. The actual permeate flow was 60% higher than the round fibers of equal length.

doi: 10.2166/wst.2018.280

In another study, Culfaz *et al.* (2011b) produced non-circular fibers that improved surface area to cross-section ratio. They concluded that the flux of membrane increased up to 16%. Wang *et al.* (2014) produced a new multi-bore HF with triangle outer geometry; the inner region to cross-sectional area ratio of this HF was more than the circular fiber and dramatically increased pure water permeability compared with the circular fibers. News (2016) proposed a new geometry to match the outer diameter of the circular fiber with the diameter of the outer circumference of the non-circular fiber. These fibers showed a 19% higher surface area and flow compared to the circular fibers. In fact, they showed that in their approach, the surface area of a fiber increases at the fixed external circumference. However, in many industries, separation and purification of the product have the highest cost. That is why finding a simpler and lower-cost separation method should be considered. There is a lot of information about the effects of operating conditions and membrane material on the membrane performance, but few studies on the influence of geometrical membrane characteristics on the filtration performance (Hashino *et al.* 2011; Shi *et al.* 2016; Sungil *et al.* 2016; Chen *et al.* 2017; Guo *et al.* 2017; Wu *et al.* 2018). Since in the past few decades, microfiltration and ultrafiltration systems have been used in various industries, such as water and wastewater treatment, it is important to gain a better understanding of their performance and the effect of various parameters on it by considering the systems' key parameter, i.e. transmembrane pressure (TMP), because of progressive fouling on the membrane (Dario *et al.* 2010). HF is typically made circular. So the following questions arise. If the HF membrane has a non-circular cross-section, what will be its performance in the process? Does it have advantages over a conventional circular HF and improve the process? What will happen if the HF has a non-circular cross-section? In the literature, there are a number of studies investigated the changing membrane characteristics but a very limited number of them have been conducted on the inner surface of the HF. Therefore, by constructing non-circular geometries, there are more choices for the shape of the fiber cross-section. Regarding the above mentioned, in most published articles, the outer surface of the fibers has changed and the internal surface remains unnoticed. Triangles, squares, rectangles and ovals have not been considered. The geometries examined in other papers have a complex form, and most of them have a smaller surface area to cross-section ratio (a) than the geometries of this paper.

The effect of the change in the surface geometry of the fiber on parameters such as the TMP has also not been investigated. Therefore, by modeling the previous works, and also for a more comprehensive examination of the subject and having a complete view, and considering the mathematical relations between geometries, three different strategies are considered in this study. The aim of this study is to investigate the performance of an HF membrane system with four internal non-circular shapes. To calculate parameters related to these geometries, three strategies have been used. The HF performance with non-circular geometries has been compared to the circular one and the effect of various parameters and operating conditions on them investigated. In this regard, two-dimensional simulations were performed using the finite element method.

METHODS

Two regions were defined for the modeling: lumen and shell regions. The lumen region is the inner part of the HF membranes and the shell region is the space between the HFs, i.e. extra capillary space (ECS) (Labecki *et al.* 1995). Since the parameters of the media are defined by their geometry, any change in geometry affects these values and the media performance. In separation processes by the HF membrane, mass conservation and mass transport equations are used. A 2D model based on solving these equations using computational fluid dynamics and finite element method using MatLab for laminar flow condition to simulate the process was used.

HF characterization and modeling

In this study, an HF sulfone polymeric membrane and UPVC inner layer module within a circular cartridge containing pressure house and dead-end HF have been studied. A Newtonian fluid with constant density and viscosity flows in the module from outside to inside, i.e. feed flows into the shell. To evaluate the performance of a full-scale system containing thousands of HFs that take part in the separation process simultaneously, the module has been assumed as a double porosity and double permeability porous medium (Mohebbi-Kalhori *et al.* 2012). The primary parameters of the model from industrial practice (Borsi & Lorain 2012) are inner radius of hollow fibers, r_i 0.15 (mm), length, L 907.5 (mm), inflow, Q_{in} 83 (l/h), outer radius of hollow fibers, r_o 0.35 (mm), number of fibers, N 3,000. Figure 1 shows the computational mesh in the simulation. As can be seen, mesh cells on the output and input of the module are smaller than the other points. The largest mesh size was 4 mm and its

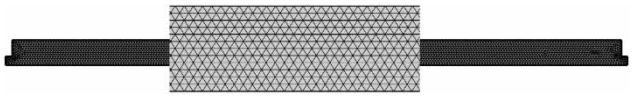

Figure 1 | Computational mesh.

smallest size was 0.15 mm and the type of mesh was triangular, and also a time-dependent modeling was used.

Strategies and determination of the HF characterization

The HF fabrication parameters affect the fiber's mechanical and transport properties, including pore morphology and permeability (Diban & Stamatialis 2014). For this reason, in this study, it has been assumed that the only permeability and porosity changes are due to the geometric parameters, and other parameters and properties are constant. Three strategies that are considered in this study are as follows: Strategy 1 (S1): the radius of the surrounding circle of non-circular geometry is equivalent to the inner radius of the circular HF; Strategy 2 (S2): the perimeter of the new geometry is equivalent to the inner region perimeter of the circular HF; Strategy 3 (S3): the radius of the inscribed circle of non-circular geometry is equivalent to the inner radius of a circular HF. In fact, inner radius in S1 and S3 are equal and only the other geometric specifications for the non-circular geometries are different. Triangle side is calculated for each strategy as follows, for example:

$$\text{S1: } \textit{Triangle side} = \frac{3r_i}{\sqrt{3}}$$

$$\text{S2: } \textit{Triangle side} = \frac{2\pi r_i}{3}$$

$$\text{S3: } \textit{Triangle side} = \frac{6r_i}{\sqrt{3}}$$

The module with triangle inner shape and cross-sections in all considered strategies are shown in Figure 2, for example.

In all three strategies, it is assumed that the non-circular HF membrane physical characteristics (porosity, pore size distribution) are similar to those of the circular one. To investigate the effect of non-circular HF on process performance, as shown in Figure 2, it is assumed that the inner shape of the HF converts to the mentioned geometry (for example, triangle in this figure) and the outer shape remains in circular HF. The geometries of the inner and outer surfaces are concentric and the outer cylinder and inner element are sufficiently long in the axial direction that the end effects can be ignored. This is due to the end effects of the finite length cylinder which produce a boundary layer that is slightly less resistant than the other regions of the cylinder; i.e. the end effects of the cylinder are ignored, so that the problem takes the form of an analysis of a cross-section for a short cylinder segment.. Because of the axial symmetry of the module and to reduce computational cost and time, a 2D model was applied.

The governing equations and boundary conditions

Darcy's law has been used for two porous media and mass transport only for the shell region, because it is assumed that pollutant does not transport in the lumen side. Governing equations are as follows (Happel 1959; Bear 1972; Mayer & Hassanizadeh 2005):

$$\nabla.q = \pm\,\Gamma \qquad \text{for each region} \tag{1}$$

$$q = -\frac{k}{\mu}\nabla p \qquad \text{for each region} \tag{2}$$

$$k_{s,x} = \frac{r_o^2}{4\varphi}\left(-log\varphi - \frac{3}{2} + 2\varphi - \frac{1}{2}\varphi^2\right) \tag{3}$$

$$k_{s,r} = \frac{r_o^2}{4\varphi}\left(-log\varphi + \frac{\varphi^2 - 1}{\varphi^2 + 1}\right),\ \varphi = 1 - \varepsilon \tag{4}$$

$$\frac{\partial}{\partial t}(\varepsilon c) + \nabla.(cq) = \nabla.(\varepsilon D\nabla c) - \alpha\Gamma(\varepsilon c) \tag{5}$$

for ECS regionb

$$\frac{\partial c_m}{\partial t} = \alpha\Gamma(\varepsilon c) \qquad \text{for ECS region} \tag{6}$$

$$R_c(c_m) = \frac{r_i}{\gamma_c} log\left(1 + \frac{1}{r_o}\left(\frac{R}{\sqrt{3\rho_c N}}\sqrt{c_m}\right)\right) \tag{7}$$

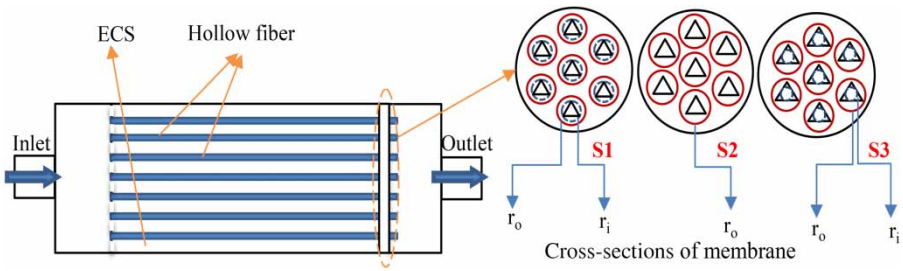

Figure 2 | Cross-section of triangle inner shape HF membrane in S1, S2, and S3.

$$R_m(c_p) = dm \frac{4A_{filt}}{N_p \pi \left(\left(\frac{c_p}{\eta}\right) - d_o^2\right)^2} \quad (8)$$

$$\text{TMP} = P_{in} - P_{out} \quad (9)$$

q is specific discharge (m/s), k is permeability of the media: $k_{s,x}$ and $k_{s,r}$ permeability for axial and radial in shell region, respectively, k_l permeability for lumen region (m^2), p pressure (kPa), φ fraction of the volume occupied by the fibers, ε porosity, c pollutant concentration (chloride in this study) in the volume of water (kg/m^3), D dispersion coefficient (m^2/s), α attachment coefficient, c_m cake concentration on membrane (kg/m^3), R_c cake resistance (m^{-1}), γ_c cake permeability (m^2), R module radius (m), ρ_c cake density (kg/m^3), R_m membrane resistance (m^{-1}), c_p mass fraction of adsorbed pollutant in membrane, A_{filt} filtering area (m^2), N_p number of pores, η adsorption constant (m^{-2}), P_{in} inlet pressure (kPa), P_{out} outlet pressure (kPa), dm membrane thickness (m), Γ rate of water loss per unit volume, μ dynamic viscosity of the water. The conditions of the solid walls were set as non-slip. The fluid flow boundary conditions include a uniform velocity at the module inlet and pressure outlet condition at the outlets of the module. The direction of velocity was parallel to the boundary. The fluid used in the modeling, was water with chloride pollutant in it (kg/m^3) and it was assumed to be Newtonian with constant density and viscosity. The density and viscosity of the medium were set as 998.2 g/m^3 and 1.003×10^{-3} Pa.s, respectively. The fluid flows into the module from the inlet and currents into the ECS from the hollow membrane porous wall. A pressure gradient was applied between the outlet and the inlet of the hollow fibers. The filtered fluid flows through the module outlet. The module houses the hollow fibers totally. In the present numerical study the boundary conditions for the mass transport used in the model are given in Table 1.

In Table 1, J is the flux (m/s), A area of module section (m^2), Q feed flow rate (l/s), R module radius (m), n normal vector outward the section, c_{in} inlet concentration of pollution. The ratio of the inner perimeter and total cross-section area (a) of the HF is equivalent to the membrane area per volume (m^2/m^3) (Culfaz Wessling *et al.* 2011b).

Table 1 | Boundary conditions

Inlet (ECS)	Outlet (lumen)
$q.n = J$	$q.n = -J$
$c = c_{in}$	$J = \frac{Q}{A}$, $A = \pi R^2$

For non-circular HF compared to circular HF, a is calculated and mentioned for all strategies in Table 2. As can be seen in S3, all geometries have a higher a than circle and triangle has the maximum value. This ratio a is an indicator of inner surface area enhancement. In fact, an inner surface of this geometry is 65% more than the circle.

$$a = \frac{\text{inner perimeter of the fiber}}{\text{total cross-sectional area of the fiber}} \quad (10)$$

To calculate porosity in the inner region of the HFs, the general definition of porosity in porous media (Bear 1972) has been used, and to calculate permeability in the inner region, Hagen–Poiseuille flow in tubes (Bear 1972; Azzouz 2004; Mayer & Hassanizadeh 2005; Mortensen *et al.* 2005; Costa 2006) has been used. According to the three mentioned strategies, the equations were calculated and are reported in Tables 3 and 4. Porosity equation for triangle shape, for example in S3, is calculated as follows:

$$\varepsilon_{lumen} = \text{Fiber number} * \frac{\text{inner surface area of fibers}}{\text{inner surface area of module}} = N * \frac{(\sqrt{3} * (\text{Triangle side})^2)/4}{\pi R^2} = \frac{3\sqrt{3}}{\pi} N \left(\frac{r_i}{R}\right)^2 \quad (11)$$

Table 2 | Inner surface to cross-section area ratio (a) in all geometries for all strategies

	a		
Geometry	**S3**	**S2**	**S1**
Triangle	1.65	1	0.83
Rectangle	1.35	1	0.9
Square	1.27	1	0.9
Ellipse	1.16	1	0.79
Circle	1	1	1

Table 3 | Lumen porosity equations for all geometries in all strategies

Geometry	S1	S2	S3
Triangle	$\frac{3\sqrt{3}}{4\pi} N \left(\frac{r_i}{R}\right)^2$	$\frac{\sqrt{3}}{9} N\pi \left(\frac{r_i}{R}\right)^2$	$\frac{3\sqrt{3}}{\pi} N \left(\frac{r_i}{R}\right)^2$
Rectangle	$\frac{1.27N}{\pi} \left(\frac{r_i}{R}\right)^2$	$2\frac{N}{\pi} \left(\frac{r_i}{R}\right)^2$	$3\frac{N\pi}{16} \left(\frac{r_i}{R}\right)^2$
Square	$\frac{2N}{\pi} \left(\frac{r_i}{R}\right)^2$	$\frac{\pi}{4} N \left(\frac{r_i}{R}\right)^2$	$\frac{4N}{\pi} \left(\frac{r_i}{R}\right)^2$
Ellipse	$1.3N \left(\frac{r_i}{R}\right)^2$	$\frac{N}{2} \left(\frac{r_i}{R}\right)^2$	$0.3N\pi \left(\frac{r_i}{R}\right)^2$

Table 4 | Lumen permeability k_l equation for all geometries in all strategies

Geometry	S1	S2	S3
Triangle	$N\frac{r_i^4}{R^2}\frac{9\sqrt{3}}{320\pi}$	$N\frac{r_i^4}{R^2}\frac{\pi^3\sqrt{3}}{1620}$	$N\frac{r_i^4}{R^2}\frac{9\sqrt{3}}{160\pi}$
Rectangle	$N\frac{r_i^4}{R^2}\frac{(2.76\pi^5-192.324)}{56\pi^6}$	$N\frac{r_i^4}{R^2}\frac{(3\pi^5-192.324)}{9216\pi^2}$	$N\frac{r_i^4}{R^2}\frac{4(1.125\pi^5-192.324)}{3\pi^6}$
Square	$N\frac{r_i^4}{R^2}\frac{(\pi^5-192.324)}{3\pi^6}$	$N\frac{r_i^4}{R^2}\frac{(\pi^5-192.324)}{192\pi^2}$	$N\frac{r_i^4}{R^2}\frac{4(\pi^5-192.324)}{3\pi^6}$
Ellipse	$N\frac{r_i^4}{40R^2}$	$N\frac{r_i^4}{R^2}\frac{(32-\pi^2)^{3/2}\pi^3}{32768}$	$N\frac{r_i^4}{4.89R^2}$

According to Darcy's law and Hagen–Poiseuille flow (Azzouz 2004; Mortensen *et al.* 2005; Costa 2006), the permeability expression is given in the following equation:

$$k_l = \frac{A}{\alpha}\frac{\varepsilon}{\tau} \tag{12}$$

α is a dimensionless geometric factor, A is the generic cross-sectional area of the HF, ε is the porosity and τ is tortuosity, which is 1 in this study. For example, permeability for triangle shape was calculated in S3:

$$\alpha = 20\sqrt{3},\ A = \frac{\sqrt{3}}{4}(\text{Triangle side})^2,$$
$$\varepsilon = N*\frac{(\sqrt{3}*(\text{Triangle side})^2)/4}{\pi R^2},$$
$$k_l = N\frac{\sqrt{3}(\text{Triangle side})^4}{320\pi R^2} \tag{13}$$

According to this equation, k_l depends on the triangle's side and it is calculated for the three strategies. For example in S3:

$$\varepsilon = \frac{3\sqrt{3}}{\pi}N(\frac{r_i}{R})^2 \Rightarrow k_l = N\frac{r_i^4}{R^2}\frac{9\sqrt{3}}{160\pi}$$

For other geometries, porosity and permeability equations are calculated similarly.

Figure 3 indicates the axial permeability of the inner region for HF for all geometries in all three strategies. Maximum and minimum values for permeability are for S3 and S1, which are related to the triangle and rectangular geometries, respectively. Also, the axial permeability for all geometries reduced from S1 to S3. It is expected that according to Darcy's law, TMP variations reduce similarly. The ratio a increased 16%, 27%, 35% and 65% in ellipse, square, rectangle and triangle geometry, respectively, in comparison with the circle. Axial permeability increased 98%, 68%, 63%, and 26% for the triangle, rectangle, ellipse, and square, respectively, in S3, in comparison to circle.

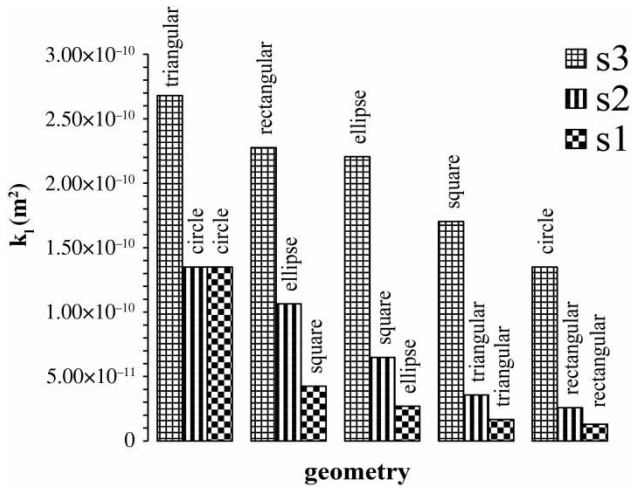

Figure 3 | The axial permeability of the inner region HF in all strategies.

RESULTS AND DISCUSSION

Model validation

In this study, an ultrafiltration (UF) module with dead-end HF at a constant flux was modeled. The validation of the model during the simulation with that of Borsi & Lorain (2012) is reported in Figure 4 and indicates a good agreement with the proposed trend mentioned by Borsi & Lorain (2012) after a few hours of runtime.

Velocity and TMP distribution

Figure 5 shows the Darcy's velocity value of the HF membrane module. As seen in this figure, there is a sharp drop and a sudden increase in the Darcy's velocity at the beginning and end parts of the module, respectively, indicating the input and output manifolds of the module, which were not porous domains, while the middle part was considered as porous medium resulting in a very low Darcy's velocity.

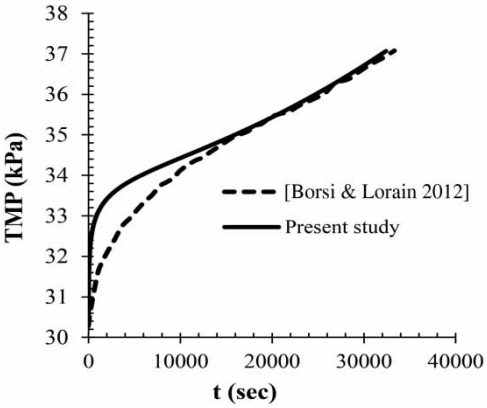

Figure 4 | Validation of present numerical model with Borsi & Lorain (2012).

After validation, geometry characteristics for non-circular cross-section HF are computed according to the mentioned three strategies and their impact on process performance are compared to circular HF during 4 days of filtration. For this purpose, TMP has been investigated for all geometries in the same conditions and also by changing the feed flow rate, feed concentration and HF number (packing density). The reduction of TMP leads to reduced energy consumption and operating costs in the industry (Ghidossi *et al.* 2006; Pearce 2008; Zhu *et al.* 2009; Howell *et al.* 2012; News 2016). As can be seen in Figure 6(a) and 6(b) in S1 and S2 there are similar and additive trends for TMP during the filtration process for all geometries. Maximum and minimum values of TMP belong to the rectangle and circle geometries (conventional HF), respectively. So in these strategies, the TMP for all considered geometries is more than that of a circle. Therefore, according to Darcy's law in porous media and as expected, pressure difference increases. So in these strategies, the system's operating costs would increase, whereas the use of HF with a circular cross-section would result in lower energy costs. Figure 6(c) shows the TMP changes versus time for all geometries in S3. As seen, all geometries have lower TMP values compared to the circle. Maximum and minimum values of TMP belong to the circle and triangle, respectively. So in this strategy, all geometries have a better performance than the circle. Consequently, using S3 to determine the HF characterization has less operating cost. Figure 6(d) compares maximum TMP after 9 hours, for all geometries in all three strategies. As shown, the lowest values of TMP are for the S3 and maximum values are for the S1. TMP decreases about 200% for the triangle HF in comparison with the circle HF; therefore operation cost is decreased in S3.

Figure 7 shows the TMP distribution in the ECS region (lumen region) using the S3 for all considered geometries compared to the circle. In this figure, the TMP was increased from inlet section to the outlet section for all considered geometries. The value of this parameter in the triangular geometry (133 kPa) is less than that of the other considered geometries.

Figure 8 shows the change in the TMP with the membrane inner surface to cross-section ratio (a) for all considered geometries in S3. Most variations are observed for triangular HF. This figure gives an example of how the TMP decrease for all considered geometries is due to the improvement of the a ratio comparing to the circle, which is the potential benefit of using the proposed geometries in this study instead of circular HF.

The effect of various operational parameters on TMP for HF with non-circular geometries

Reduction of energy consumption was achieved by changing the circular HF geometry, as proposed in the present study. To continue in this section, the feed concentration, flow rate, and packing density are investigated as the most

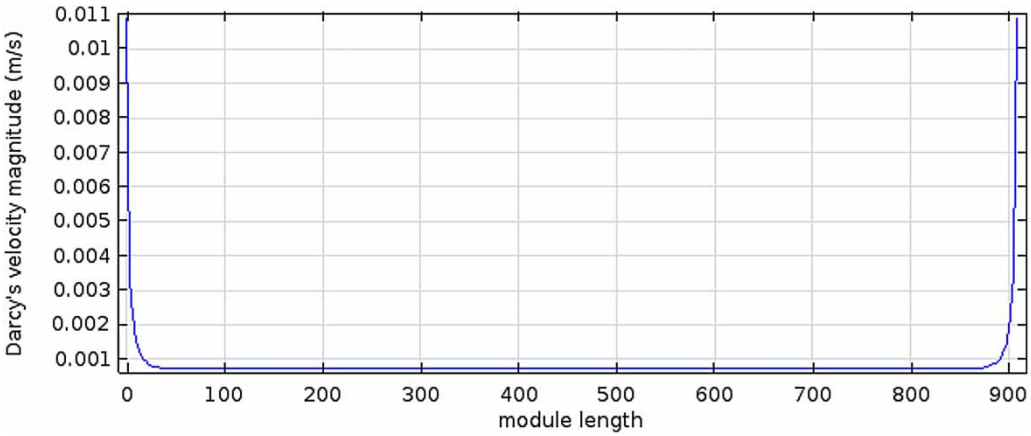

Figure 5 | The Darcy's velocity magnitude in the module.

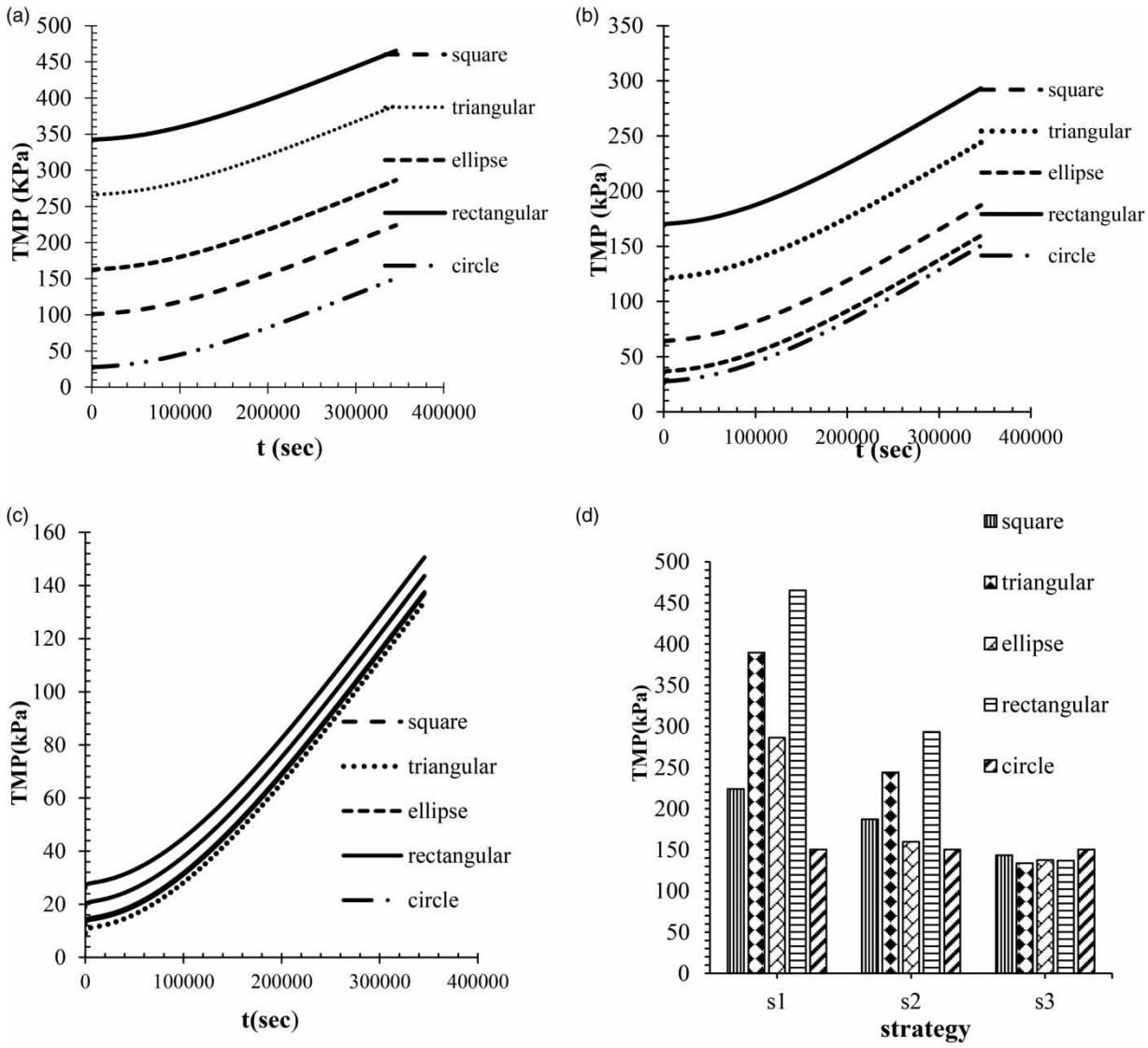

Figure 6 | Comparison of TMP changes in all geometries in S1 (a), S2 (b) and S3 (c), and maximum TMP for all geometries in all strategies (d).

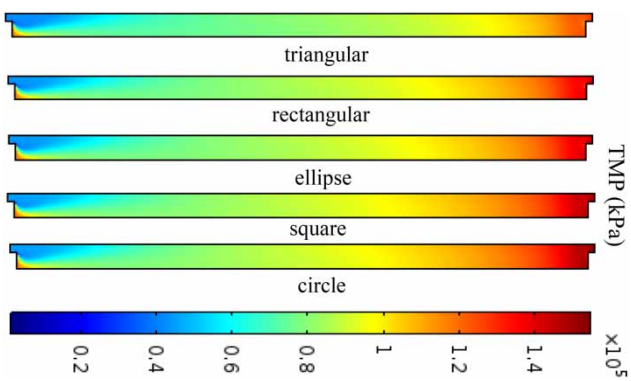

Figure 7 | Comparison of the pressure difference between ECS and lumen and TMP in the S3 for all considered geometries.

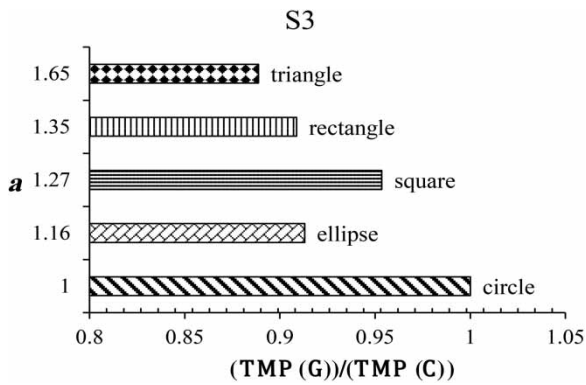

Figure 8 | Comparison of maximum TMP and *a* in S3 compared to circle. (C) circle; (G) other geometries.

important parameters affecting the performance of the HF membrane modules.

The effect of feed concentration

For this purpose, the effect of three different feed concentrations (0.35, 0.45, 0.6 kg/m^3) on the TMP variations were investigated. Because of observing a similar trend in the TMP variations in all three strategies, and also the advantage of S3 compared to the two other strategies according to the previous sections, the results of this strategy have been discussed only. As expected and shown in Figure 9(a), increasing (or decreasing) of the concentration would increase (or decrease) the TMP value in all considered strategies and geometries. The reason is that an increase in feed concentration changes the solution viscosity, which affects the energy consumption (Garcia & Chiu 2008) and creates a stiffer layer on the membrane surface. An additional layer causes an increase in the resistance for the water transport (Luo *et al.* 2015) and, as shown, the TMP increases as well.

The effect of HF number (packing density)

The packing density can be decreased by decreasing the number of HFs per bundle, which affects hydrodynamic conditions (Bütehorn 2011). To evaluate this effect, HF number was reduced to 2,000 and TMP variation investigated. As expected and shown in Figure 9(b), similar to a circle, reducing of the HF numbers leads to increase in TMP due to the inner surface to cross-section ratio reduction. Results show in the same packing density, for different geometries, the TMP decreases in S1 and S2 and increases in S3 compared to the circle.

The effect of feed flow rate

In order to evaluate the effect of feed flow rate on the process performance, this parameter was decreased to 50%. Due to the feed velocity reduction, the TMP decreases (Ghidossi *et al.* 2006; Peng *et al.* 2011) in all strategies and all geometries and leads to reduced energy consumption (Pearce 2008). As shown, the TMP variation is not equal for all geometries. According to Figure 10, a maximum reduction is 85% corresponding to rectangular HF in S1, and minimum reduction in the TMP is 55% corresponding to the triangle HF in S3. Therefore, for different geometries, the TMP variation is affected by the reduction in the feed flow rate at the same conditions.

CONCLUSIONS

HF membranes are extensively used in the separation processes due to their dense size and capability to do separations that may not be technically or economically practicable via other technologies. In the present study, a set of modeling and simulations were done to evaluate the effect of the changes in the geometry of the inner surface of HF membrane with the same intrinsic properties used in the water and wastewater treatment. In this regard, three strategies and five geometries (circle, triangle, ellipse, square, and rectangle) were introduced to calculate the geometric parameters of the HF membrane. Using S1 and S2 showed that the inner surface area to cross-section ratio (a) in all cases was less than that of the circle, while in the S3, this ratio was significantly high. In S3, a maximum

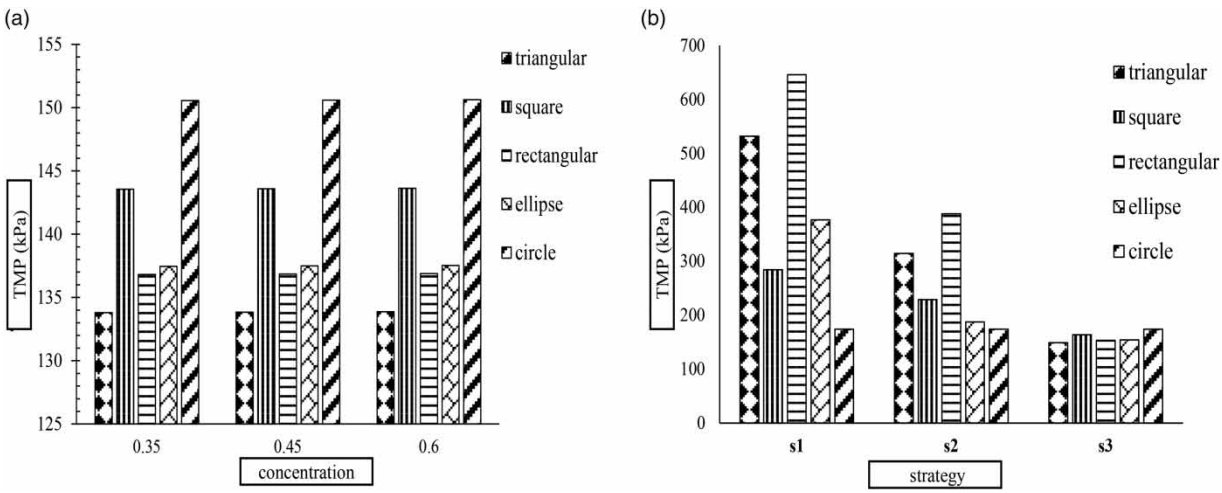

Figure 9 | TMP changes via concentration in S3 (a). Comparison of the TMP in all considered geometries and strategies by reducing the HF number (b).

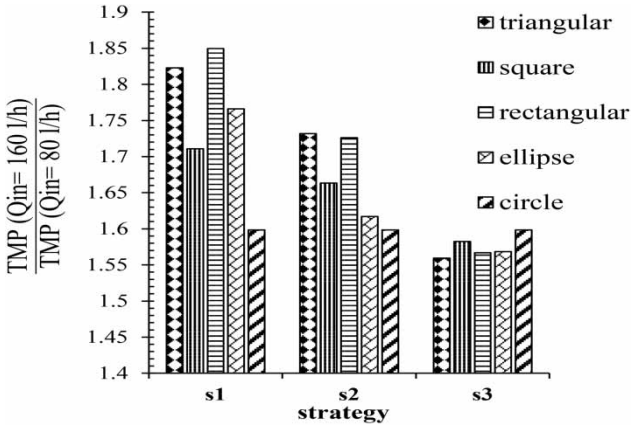

Figure 10 | The TMP variations by 50% reduction of the feed flow rate.

ratio *a* was 65% corresponding to the triangle. Also, the axial permeability for all considered geometries was greater than the circular HF. The ratio *a* increased 16%, 27%, 35% and 65% in ellipse, square, rectangle, and triangle geometry, respectively, in comparison to circle. Axial permeability increased 98%, 68%, 63%, and 26% for the triangle, rectangle, ellipse, and square respectively in S3 in comparison to the circle.

The study revealed that the TMP variations for the circle geometry were minimum in the S1 and S2 and maximum in S3. In other considered geometries these variations were as follows:

$$TMP_{square} > TMP_{triangle} > TMP_{ellipse} > TMP_{rectangle} > TMP_{circle} \quad (S1)$$

$$TMP_{square} > TMP_{triangle} > TMP_{ellipse} > TMP_{rectangle} > TMP_{circle} \quad (S2)$$

$$TMP_{circle} > TMP_{square} > TMP_{ellipse} > TMP_{rectangle} > TMP_{triangle} \quad (S3)$$

Changes in feed flow rate in the different geometries made unequal TMP variations. The maximum TMP reduction was 85% corresponding to HF with rectangle inner cross-section geometry in the S1 due to 50% feed flow rate reduction, and the minimum was 55% corresponding to the triangle in S3. In addition, the TMP variations were because of changes in the HF inner surface to the cross-section ratio and axial permeability. The obtained results showed that increasing the permeability would reduce the pressure drop, which was in accordance with Darcy's law in the porous media. Moreover, one of the most important advantages of the TMP reduction is to reduce the system's energy consumption and operating cost as well. The results showed that using the S3 for the HF characterization can improve the separation process performance, by increasing the inner surface to the cross-section ratio, and also decreasing TMP. The TMP decreases nearly 200% when the HF membrane geometry changes from a round inner shape to a triangle one. These findings quantitatively demonstrate the advantages of the non-circular inner shape HF membranes over the traditional round inner shape ones. Therefore, using these kinds of HF membrane is recommended for the separation process such as in water and wastewater treatment, especially for the wastewater manager or controller who focuses on operating-cost savings.

REFERENCES

Arthanareeswaran, G., Mohan, D. & Raajenthiren, M. 2010 Preparation, characterization and performance studies of ultrafiltration membranes with polymeric additive. *Journal of Membrane Science* **350**, 130–138. doi: 10.1016/j.memsci.2009.12.020.

Azzouz, H. 2004 *The Dependence of the Cross-Sectional Shape on the Hydraulic Resistance of Microchannels, MIC*. Department of Micro and Nanotechnology, Technical University of Denmark, Kongens Lyngby, Denmark.

Bear, J. 1972 *Dynamics of Fluids in Porous Media*. Elsevier, New York.

Borsi, I. & Lorain, O. 2012 A space-averaged model for hollow fibre membranes filters. *Journal of Computers and Chemical Engineering* **39**, 65–74. doi: 10.1016/j.compchemeng.2011.12.017.

Buer, T. & Cumin, J. 2010 MBR module design and operation. *Desalination* **250**, 1073–1077.

Bütehorn, S. 2011 *Experimental and Numerical Investigation of the Hydrodynamics of Microfiltration Processes Using a Multi-Scale Approach*. PhD thesis. Rheinisch-Westfälischen Technischen Hochschule (RWTH), Aachen, Germany.

Chen, X., Su, Y., Aydin, D., Zhang, X., Ding, Y. & Reay, D. 2017 Experimental investigations of polymer hollow fibre integrated evaporative cooling system with the fibre bundles in a spindle shape. *Energy and Buildings* **154**, 166–174. doi: 10.1016/j.cep.2018.01.003.

Costa, A. 2006 Permeability-porosity relationship: a reexamination of the Kozeny-Carman equation based on a fractal pore-space geometry assumption. *Geophysical Research Letters* **33** (2), doi: 10.1029/2005GL025134.

Culfaz, P. Z., Buetehorn, S., Utiu, L., Kueppers, M., Bluemich, B., Melin, T. & Lammertink, R. G. H. 2011a Fouling behavior of microstructured hollow fiber membranes in dead-end filtrations: critical flux determination and NMR imaging of particle deposition. *American Chemical Society, Langmuir* **27** (5), 1643–1652. doi:doi:10.1021/la1037734.

Culfaz, P. Z., Wessling, M. & Lammertink, R. G. H. 2011b Hollow fiber ultrafiltration membranes with microstructured inner

skin. *Journal of Membrane Science* **369**, 221–227. doi: 10.1016/j.memsci.2010.11.063.

Dario, F., Liberti, L. & Notarnicola, M. 2010 Ultrafiltration (UF) pilot plant for municipal wastewater reuse in agriculture: impact of the operation mode on process performance. *Water* **2** (4), 872–885. doi: 10.3390/w2040872.

Deng, J., Zhang, Y., Liu, J. & Zhang, H. 2011 Preparation of three-bore hollow fiber charged nanofiltration membrane for separation of organics and salts. *Water Science and Technology* **65** (1), 171–176. doi: 10.2166/wst.2011.851.

Diban, N. & Stamatialis, D. 2014 Polymeric hollow fiber membranes for bioartificial organs and tissue engineering applications. *Journal of Chemical Technology and Biotechnology* **89** (5), 633–643. doi: 10.1002/jctb.4300.

EPA 2005 *Membrane Filtration Guidance Manual*. Office of Water, United States Environmental Protection Agency, Washington, DC.

Garcia, F. & Chiu, T. 2008 Economic aspects of critical flux operability in star shaped microfiltration membranes: influence of some operating conditions. *Journal of Membrane Science* **325**, 641–646. doi: 10.1016/j.memsci.2008.08.033.

Ghidossi, R., Daurelle, J. V., Veyret, D. & Moulin, P. 2006 Simplified CFD approach of a hollow fiber ultrafiltration system. *Chemical Engineering Journal* **123** (3), 117–125. doi: 10.1016/j.cej.2006.07.007.

Guo, X., Wang, Y., Zhang, H., Li, P. & Ma, C. 2017 Numerical and experimental investigation for cleaning process of submerged outside-in hollow fiber membrane. *Water Science and Technology* **76** (6), 1283–1299. doi: 10.2166/wst.2017.228.

Happel, J. 1959 Viscous flow relative to arrays of cylinders. *AIChE Journal* **5**, 174–177. doi: 10.1002/aic.690050211.

Hashino, M., Katagiri, T., Kubota, N., Ohmuki, Y., Maruyama, T. & Matsuyama, H. 2011 Effect of surface roughness of hollow fiber membranes with gear-shaped structure on membrane fouling by sodium alginate. *Journal of Membrane Science* **366**, 389–397. doi: 10.1016/j.memsci.2010.10.025.

Howell, J., Sanchez, V. & Field, R. W. eds. 2012 *Membranes in Bioprocessing: Theory and Applications*. Springer Science & Business Media, Berlin.

Jiang, L. Y., Chung, T. S. & Rajagopalan, R. 2008 Dehydration of alcohols by pervaporation through polyimide matrimid (R) asymmetric hollow fibers with various modifications. *Chemical Engineering Science* **63**, 204–216. doi: 10.1016/j.ces.2007.09.026.

Labecki, M., Piret, J. M. & Bowen, B. D. 1995 Two-dimensional analysis of fluid flow in hollow-fibre modules. *Chemical Engineering Science* **50** (21), 3369–3384. doi: 10.1016/0009-2509(95)00185-8.

Luo, L., Han, G., Chung, T. S., Weber, M., Staudt, C. & Maletzko, C. 2015 Oil/water separation via ultrafiltration by novel triangle-shape tri-bore hollow fiber membranes from sulfonated polyphenylenesulfone. *Journal of Membrane Science* **476**, 162–170. doi: 10.1016/j.memsci.2014.11.035.

Mayer, A. & Hassanizadeh, S. (eds) 2005 *Soil and Groundwater Contamination: Nonaqueous Phase Liquids*. Water Resources Monograph 17, American Geophysical Union, New York.

Mohebbi-Kalhori, D., Behzadmehr, A., Doillon, C. J. & Hadjizadeh, A. 2012 Computational modeling of adherent cell growth in a hollow-fiber membrane bioreactor for large-scale 3-D bone tissue engineering. *Journal of Artificial Organs* **15** (3), 250–265. doi: 10.1007/s10047-012-0649-1.

Mortensen, A., Okkels, F. & Bruus, H. 2005 Reexamination of Hagen-Poiseuille flow: shape dependence of the hydraulic resistance in microchannels. *Physical Review E. Statistical, Nonlinear, and Soft Matter Physics* **71** (5), 1–4. doi: 10.1103/PhysRevE.71.057301.

News 2016 GE UF modules reduce operating costs and increase energy efficiency. *Membrane Technology* **26** (9), 2–3. doi: 10.1016/S0958-2118(16)30181-1.

Pearce, G. K. 2008 A cost optimization study of flux and fouling rate for UF in the water industry. *Water Science and Technology, Water Supply* **8** (1), 113–120. doi: 10.2166/ws.2008.004.

Peng, N., Teoh, M. M., Chung, T. S. & Ling Koo, L. 2011 Novel rectangular membranes with multiple hollow holes for ultrafiltration. *Journal of Membrane Science* **372**, 20–28. doi: 10.1016/j.memsci.2011.01.022.

Shi, H., Xue, L., Gao, A. & Zhou, Q. 2016 Dual layer hollow fiber PVDF ultra-filtration membranes containing Ag nano-particle loaded zeolite with longer term anti-bacterial capacity in salt water. *Water Science and Technology* **73** (9), 2159–2167. doi: 10.2166/wst.2016.062.

Sungil, J., Rajabzadeh, S., Okamura, R., Ishigami, T., Hasegawa, S., Kato, N. & Matsuyama, H. 2016 The effect of membrane material and surface pore size on the fouling properties of submerged membranes. *Water* **8** (12), 602. doi: 10.3390/w8120602.

Wan, C. F., Yang, T., Lipscomb, G. G., Stookey, D. J. & Chung, T. S. 2017 Design and fabrication of hollow fiber membrane modules. *Journal of Membrane Science* **538**, 96–107. doi: 10.1016/j.memsci.2017.05.047.

Wang, P., Luo, L. & Chung, T. S. 2014 Tri-bore ultra-filtration hollow fiber membranes with a novel triangle-shape outer geometry. *Journal of Membrane Science* **452**, 212–218. doi: 10.1016/j.memsci.2013.10.033.

Widjojo, N. & Chung, T. S. 2006 Thickness and air gap dependence of macrovoid evolution in phase-inversion asymmetric hollow fiber membranes. *Industrial & Engineering Chemistry Research* **45**, 7618–7626. doi: 10.1021/ie0606587.

Wu, S. E., Lin, Y. C., Hwang, K. J., Cheng, T. W. & Tung, K. L. 2018 High-efficiency hollow fiber arrangement design to enhance filtration performance by CFD simulation. *Chemical Engineering and Processing: Process Intensification* **125**, 87–96. doi: 10.1016/j.cep.2018.01.003.

Zhu, A., Christofides, P. D. & Cohen, Y. 2009 Energy consumption optimization of reverse osmosis membrane water desalination subject to feed salinity fluctuation. *Industrial & Engineering Chemistry Research* **48** (21), 9581–9589. doi: 10.1021/ie900729x.

First received 1 December 2017; accepted in revised form 11 June 2018. Available online 26 June 2018